Characterization of Reaction Pathways on the Potential Energy Surfaces for H + SO_2 and HS + O_2

A. Goumri, John-David R. Rocha, Dianna Laakso, C. E. Smith, and Paul Marshall*

Department of Chemistry, University of North Texas, P.O. Box 305070, Denton, Texas 76203-5070

Received: July 15, 1999; In Final Form: October 22, 1999

Unimolecular pathways for the isomerization and/or dissociation of HSOO, HOSO, HSO_2, and HOOS to H + SO_2 and OH + SO have been investigated computationally, as well as HSO formation via an HSOO intermediate. The atmospheric lifetime of HSO_2 is discussed. Some pathways have no barrier, including OH + SO → HOSO and H + SOO → HSOO and SOOH, while structures and vibrational frequencies of transition states for HOSO → H + SO_2, HOOS → OH + SO, HOSO → HSO_2, HSOO → HS + O_2, and HSO_2 → H + SO_2 have been characterized at the MP2=FULL/6-31G(d) level. Some geometries were further refined at the QCISD/6-311G(d,p) level. Gaussian-2 theory was employed to calculate approximate QCISD(T)/6-311+G-(3df,2p) energy barriers, and the kinetics were analyzed by RRKM theory. Rate constant expressions at the high and low-pressure limits and thermochemical properties for transient intermediates are tabulated, and the results are discussed in the context of atmospheric and combustion chemistry. A revised theoretical H−OSO bond strength is compatible with the flame data for SO_2-catalyzed recombination of H atoms.

I. Introduction

There are very few experimental studies of species of the stoichiometry "HSO_2", despite their importance in combustion and atmospheric chemistry. No spectroscopic data are available apart from the results obtained by McDowell et al.,[1] who examined the addition of H to SO_2 in a frozen Kr matrix and concluded that H bonds to S to form HSO_2. This species, together with HOSO where H is bonded to O, is thought to be responsible for catalytic removal of atomic hydrogen in sulfur-seeded flames via the sequence[2−7]

$$H + SO_2 \rightarrow \text{adduct}$$

$$\text{adduct} + H \rightarrow SO_2 + H_2$$

and binding energies between 200 and 264 kJ mol^{-1} have been derived from flame modeling. "HSO_2" has also been proposed as the product of HSO oxidation by O_3 and NO_2[8,9] and may therefore play a role in the atmospheric oxidation of sulfur species. HOSO and HSO_2 have very recently been identified, in a neutralization−reionization experiment with mass spectrometric detection, by Tureček and co-workers.[10,11] By analogy with the observed formation of an adduct between CH_3S and O_2, the HSOO species has been proposed, although never detected.[12] The aim of the present work is to improve our understanding of sulfur oxidation mechanisms, through computational investigations of the thermochemistry and kinetics of adducts on the H/S/O/O potential energy surface (PES). This PES may assist the interpretation of experiments such as those by Morris et al., who reacted translationally hot H atoms with SO_2 and observed time-resolved infrared chemiluminescence from OH.[13]

The first ab initio studies of HSO_2 and HOSO were by Boyd et al.,[14] who found HOSO to be the more stable isomer, and Hinchliffe,[15] who focused on HSO_2. Binns and Marshall[16] carried out geometry optimizations for these molecules plus two transition states (TSs) on the H + SO_2 PES at the MP2=FULL/3-21G(d) level of theory, (and in some cases with a larger basis) followed by single-point energy calculations with the double-ζ plus polarization 6-31G(d) basis set and corrections for the effects of electron correlation with MP4 perturbation theory. HSO_2 is included in a computational review of sulfur compounds by Basch and Hoz.[17] Morris and Jackson[18] characterized HSO_2 and HOSO at the MP4/DZP//MP2/DZP level, while we have published an investigation of these two molecules plus HSOO and HOOS carried out with Gaussian-2 (G2) theory, and focused on their thermochemistry.[19] The G2 methodology has a target accuracy of ±8 kJ mol^{-1} for atomization enthalpies and an average absolute deviation of 5 kJ mol^{-1} for a set of 55 test molecules[20−22] and yields approximate QCISD(T)/6-311+G-(3df,2p) energies. These results for bound minima were combined with empirically estimated barrier heights in a recent flame mechanism by Glarborg et al.[23] Very recently, Qi et al. published MP2/6-311G(d,p) values for the geometries, frequencies, and energies in the H + SO_2 system[24] and Tureček et al.[11] used G2(MP2) theory to investigate neutral and ionic HSO_2 species and transition states.

Here we apply G2 theory to the PES that controls the kinetics of H + SO_2 and HS + O_2 and the behavior of the resulting adducts. TS geometries are fully optimized with MP2=FULL/6-31G(d) and in some cases QCISD/6-311G(d,p) theory and their vibrational frequencies obtained, to predict rate constants for addition, dissociation, and isomerization via RRKM calculations. A preliminary study of SH + O_2 kinetics has already been reported.[25] The results are discussed in the context of atmospheric and combustion chemistry.

II. Ab Initio Methodology

The general principles of quantitative molecular orbital theory have been described elsewhere,[26,27] and the ab initio calculations were carried out with the GAUSSIAN 90, 92, and 94

* Corresponding author. E-mail: marshall@unt.edu.

10.1021/jp9924070 CCC: $18.00
Published on Web 12/07/1999

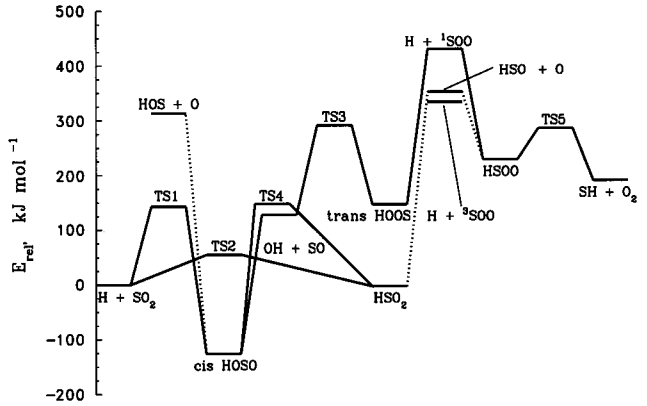

Figure 1. Potential energy diagram calculated at the MP2=FULL/6-31G(d) level, showing energies (excluding ZPE) relative to H + SO_2.

programs.[28−30] Preliminary searches of the doublet PES were made at the self-consistent field or Hartree−Fock (HF) and second-order Mφller−Plesset (MP2) levels of theory with the 3-21G(d) and 6-31G(d) basis sets and spin-unrestricted (UHF) wave functions. The MP2 calculations incorporate a partial correction for the effects of electron correlation. Each TS geometry was verified to have a single imaginary frequency at the MP2=FULL/6-31G(d) level. The reactants and products connected by each TS were confirmed by following the intrinsic reaction coordinate at the HF/6-31G(d) level. The calculated harmonic frequencies were scaled by a standard factor of 0.95[31] to account partly for effects of basis set deficiency and anharmonicity and were used to derive the zero-point vibrational energy ZPE. The stability of the wave function with respect to relaxation of internal constraints[32] was verified for each stationary point. Some TSs, discussed in section III.3, were not well described at the MP2 level, as evidenced either by high degrees of spin-contamination or unrealistic vibrational frequencies. When it appeared that HF or MP2 methods were breaking down, the geometry was refined at the QCISD/6-311G(d,p) level of theory, essentially the G2Q method of Durant and Rohlfing[33] but without the QCISD frequencies that are expensive computationally because analytic second derivatives are unavailable.

The next step was to obtain energies at a much higher level of theory. Approximate QCISD(T)/6-311+G(3df,2p) energies were calculated at the MP2=FULL/6-31G(d) geometries by means of the G2 methodology,[22] where the MP4/6-311G(d,p) energy was augmented with a series of additive corrections. Use of MP2 rather than HF frequencies to obtain the ZPE is a modification of the original G2 method; we have summarized the slightly altered energies of relevant one-, two- and three-atom species elsewhere.[19]

III. Results and Discussion

III.1. Geometries and Vibrational Frequencies. The structures and frequencies of the molecules HSO_2, HOSO, HSOO, and HOOS and the fragments SOO, HSO, and HOS have been discussed earlier.[19,25,34] Pathways that connect these minima are summarized on Figure 1, which represents the PES searched at the MP2=FULL/6-31G(d) level. Transition states for the following processes have been characterized at this level; the geometries are shown in Figure 2, and the scaled vibrational frequencies are listed in Table 1.

$$\mathrm{HOSO\ (+M) \rightarrow H + SO_2\ (+M)} \qquad (1)$$

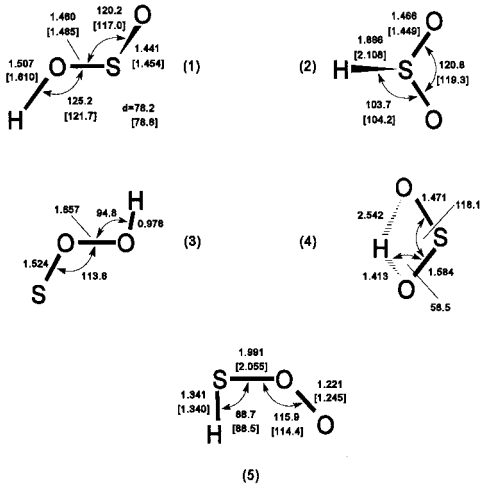

Figure 2. MP2=FULL/6-31G(d) geometries for transition states on the doublet H/S/O/O PES: (1) TS1 for HOSO → H + SO_2; (2) TS2 for HSO_2 → H + SO_2; (3) TS3 for HOOS → OH + SO; (4) TS4 for HOSO → HSO_2; (5) TS5 for HSOO → HS + O_2. Distances are in angstroms and angles are in degrees. QCISD/6-311G(d,p) data are shown in square brackets.

TABLE 1: Scaled MP2=FULL/6-31G(d) Frequencies, in cm^{-1}, for Transition States on the H + SO_2 PES

TS1		TS2		TS3		TS4		TS5	
sym	ν	sym	ν^a	sym	ν	sym	ν	sym	ν
A	2641i	A′	1063i	A′	1175i	A	1719i	A′	905i
A	298	A″	347	A″	98	A	407	A″	113
A	500	A′	358	A′	331	A	639	A′	385
A	609	A′	517	A′	884	A	854	A′	805
A	1218	A′	1177	A′	1125	A	1216	A′	1395
A	1527	A″	1381	A′	3554	A	2191	A′	2635

[a] Unscaled Brueckner frequencies (see text).

$$\mathrm{HSO_2\ (+M) \rightarrow H + SO_2\ (+M)} \qquad (2)$$

$$\mathrm{HOOS\ (+M) \rightarrow OH + SO\ (+M)} \qquad (3)$$

$$\mathrm{HOSO\ (+M) \rightarrow HSO_2\ (+M)} \qquad (4)$$

$$\mathrm{HSOO\ (+M) \rightarrow HS + O_2\ (+M)} \qquad (5)$$

The TS for reaction 2, TS2, is poorly described by MP2 theory. Qi et al. published frequencies including an impossibly high value above 9000 cm^{-1}.[24] Uncorrected, this would lead to a large error in the ZPE of around 40 kJ mol^{-1}. We confirm similar difficulties using analytic MP2 and finite-difference QCISD frequencies with a variety of basis sets. The trouble arises with the higher frequency A″ mode that breaks the C_s symmetry of TS2, which exhibits an "instability volcano" in the underlying Hartree−Fock wave function.[35] Properties derived via algorithms that conserve symmetry, such as the geometry and energy, are unaffected. To derive the ZPE we instead employed frequencies obtained via Brueckner theory at the B-CCD/6-31G(d) level.[36,37] This happened to yield frequencies close to the HF/6-31G(d) values when the latter were scaled by the usual factor of 0.893.[26]

There are apparently no barriers, at the MP2=FULL/6-31G(d) level, to the three reactions

$$\mathrm{OH + SO\ (+M) \rightarrow HOSO\ (+M)} \qquad (6)$$

$$\mathrm{H + SOO\ (+M) \rightarrow HOOS\ (+M)} \qquad (7)$$

$$\mathrm{H + SOO\ (+M) \rightarrow HSOO\ (+M)} \qquad (8)$$

The reaction pathways

$$HOSO\ (+M) \rightarrow HOS + O\ (+M) \quad (9)$$

$$HSO_2\ (+M) \rightarrow HSO + O\ (+M) \quad (10)$$

$$HSOO\ (+M) \rightarrow HSO + O\ (+M) \quad (11)$$

are shown as dotted lines on Figure 1 because the presence of distinct TSs is unclear.[38] No TS has been located for SOOH → HSOO isomerization, although our preliminary indications are that if a TS exists it has an energy close to that of H + SOO. All attempts to locate a TS for HSOO isomerization to HSO_2 led instead to the dissociation products HSO + O. We note that Morris and Jackson[18] argue for the absence of any TS for reactions 9 and 10. G2 energies of the TSs are presented in Table 2.

III.2. Thermochemistry. The room-temperature thermochemistry of HSO_2, HOSO, HOOS, HSOO, and SOO has been analyzed earlier and discussed in the context of atmospheric and combustion chemistry.[19,25] The conclusions were that HOSO and perhaps HSO_2 are sufficiently stable to participate as intermediates in sulfur-containing flames. However, the predicted bond strengths of 162.6 kJ mol^{-1} in H−OSO and 62.6 kJ mol^{-1} in H−SO_2 (see Figure 3),[19] are significantly lower than the values between 200 and 264 kJ mol^{-1} suggested from flame models.[3−5] Both HSOO and HSO_2 could be formed by exothermic reactions of HSO with O_3, but only HSO_2 is accessible from HSO + NO_2 or N_2O.[39,40] The HS−OO bond energy was calculated to be 31.5 kJ mol^{-1}, low enough to make adduct formation between SH and O_2 unfavorable at room temperature but not at lower temperatures. HOOS was predicted to be 14.9 kJ mol^{-1} endothermic with respect to SO + OH at 298 K, and therefore can only be stable if there is a significant barrier to this dissociation. Here, we present thermochemical data for HSO_2, HOSO, and HSOO extended over 200−2000 K, which properly take account of the hindered internal rotors in the latter three molecules, in Tables 3−5. These data were employed to calculate the equilibrium constants required in the kinetic analysis below.

III.3. Kinetics. Figure 3 illustrates the vibrationally adiabatic potential energy surface at 0 K, based on G2 enthalpies relative to H + SO_2. This diagram may be contrasted to Figure 1, derived with a much smaller basis set and a lower level of correlation correction. The main qualitative difference is that the energies of several MP2=FULL/6-31G(d) transition states are significantly lowered relative to the reactants and products they connect. In some cases, the TS energy now falls between that of the reactants and products, which suggests there may be no energy barrier to these processes in the exothermic direction. Thus, there is no apparent barrier to the dissociation of HOOS. The PES at this geometry is flat, and stretching the central O−O bond from 1.46 to 1.66 Å decreases the G2 energy by only about 3 kJ mol^{-1}. The potential energy before inclusion of ZPE suggests a weakly bound molecule, but the existence of a distinct HOOS species is doubtful because the calculated SO to OH binding energy is comparable to or less than the zero-point vibrational energy for O−O stretching in HOOS. We therefore do not consider HOOS further.

The unimolecular kinetics of the dissociation or isomerization of reagent molecules were analyzed in terms of RRKM theory, as detailed for example by Gilbert and co-workers.[41,42] The general Lindemann−Hinshelwood mechanism for this class of reaction can be summarized as

$$A + M \rightleftharpoons A^* + M$$

$$A^* \rightarrow \text{product(s)}$$

At low pressures, the first step, energy transfer from the bath gas M to A to form internally excited A*, is rate limiting and the overall rate of formation of product(s) is proportional to pressure. The kinetics are described by the low-pressure second-order rate constant k_0, and the reaction rate is k_0[M][A]. At high [M], the second step is rate-limiting and the reaction rate is described by k_∞[A], where k_∞ is the first-order rate constant at the high-pressure limit. Thus, the effective pseudo-first-order rate constant for formation of product(s), k_{ps1}, is proportional to [M] at low pressures and reaches a limiting value of k_∞ at high pressures. The intermediate "fall-off" regime is where $k_{ps1} \approx k_\infty/2$, and this regime moves to higher [M] as the temperature is raised.

RRKM rate constants take account of the internal energy distribution of A* and conservation of angular momentum, and are derived here in two ways. The first method, "A", is applicable to reactions where there is a clear maximum along the reaction coordinate, which is identified as the TS. An example is reaction 1 where Figure 3 shows a significant barrier beyond the endothermicity for breaking the H−O bond in HOSO. For this kind of PES, the vibrational and rotational partition functions of the "tight" TS, where bonds are modestly extended with respect to the reactant,[43] were calculated straightforwardly from the ab initio data in Figure 1 and Table 1. RRKM calculations were carried out with the UNIMOL program[42] for an Ar bath gas, on the assumption of a weak collision "exponential down" model for energy transfer between the bath gas and species of stoichiometry HSO_2. $\sigma = 3.81$ Å and $\epsilon/k_B = 185$ K were chosen as the averaged Lennard-Jones parameters that describe collisions with the bath gas, based on the suggested values for Ar and HSO_2.[44] The reactant molecule and the TS are usually close to symmetric tops, and effects of angular momentum conservation on changes in rotational energy during the course of reaction were taken into account by allowing the energy of the one-dimensional external rotational mode with the unique moment of inertia to be "active",[41] i.e., available to help cross the potential barrier. The other two rotations were taken to be inactive and were combined in a two-dimensional external rotational mode. The kinetic results were multiplied by a tunneling factor Γ defined by the simple Wigner expression,[45]

$$\Gamma \approx 1 + \frac{1}{24}\left(\frac{h\nu_i^*}{k_B T}\right)^2 \quad (12)$$

where ν_i is the imaginary frequency for motion along the reaction coordinate, calculated at the MP2=FULL/6-31G(d) level. This expression for Γ will not be accurate when the degree of tunneling is large.

Rate constants for back reactions were obtained via microscopic reversibility, using equilibrium constants based on data in Tables 3−5 and the JANAF Tables.[39] An exception is SH, because we were unable to reproduce the JANAF temperature dependence of $\Delta_f H$(SH) from C_p and ancillary data. Instead we employed the variation of $\Delta_f H$(SH) quoted in the Texas A&M tables,[46] that is in accord with the C_p results, together with the value $\Delta_f H_0$(SH) = 142.5 ± 3.0 kJ mol^{-1} derived kinetically,[47] that agrees within the experimental uncertainty with spectroscopic determinations.[48,49] Of course, forward and reverse reactions exhibit the same pressure dependence.

For dissociation reactions such as (5) that proceed without explicit barriers beyond the endothermicity, assignment of the TS was made using an alternative procedure, "B", based on canonical variational transition state theory. Trial points along

TABLE 2: Absolute G2 Energies of Transition States on the H + SO_2 PES Calculated at the MP2=FULL/6-31G(d) Optimized Geometries

species	sym	state	MP4/6-311G(d,p)[a]	$\langle S^2\rangle$ [b]	$\Delta E(+)$[c]	ΔE(2df)[c]	ΔE(QCI)[c]	ΔE(ZPE)[c]	Δ[c]	E(G2)[a]	H_{rel}[d]
TS1	C_1	^{2}A	−548.26488	1.087	−15.10	−161.16	−10.54	9.46	−14.92	−548.50233	37.6
TS1[e]	C_1	^{2}A	−548.26203	1.197	−14.86	−161.16	−15.54	9.46	−14.45	−548.50337	34.9
TS2	C_s	^{2}A′	−548.29616	0.889	−14.18	−162.02	5.12	8.61[f]	−15.26	−548.51909	−6.4
TS2[e]	C_s	^{2}A′	−548.29492	0.839	−13.79	−160.78	8.33	8.61[f]	−15.53	−548.51327	8.9
TS3	C_s	^{2}A″	−548.24826	0.762	−15.42	−134.75	−25.65	13.65	−10.85	−548.46646	131.7
TS4	C_1	^{2}A	−548.27660	0.819	−15.20	−157.42	−0.56	12.09	−15.24	−548.49812	48.6
TS5	C_s	^{2}A″	−548.23855	1.338	−10.71	−128.13	−16.52	12.21	−10.53	−548.43742	208.0
TS5[e]	C_s	^{2}A″	−548.23804	1.434	−10.55	−127.18	−17.26	12.21	−10.46	−548.43647	210.5

[a] In atomic units (1 au ≈ 2625.3 kJ mol^{-1}). [b] For the HF/6-311G(d,p) wave function. [c] Component of G2 energy in 10^{-3} au. $n_{pair} = 9$ and $n_{unpair} = 1$. [d] G2 Enthalpy relative to H + SO_2 at 0 K, in kJ mol^{-1}. [e] At the QCISD/6-311G(d,p) geometry. [f] Brueckner CCD/6-31G(d) ZPE.

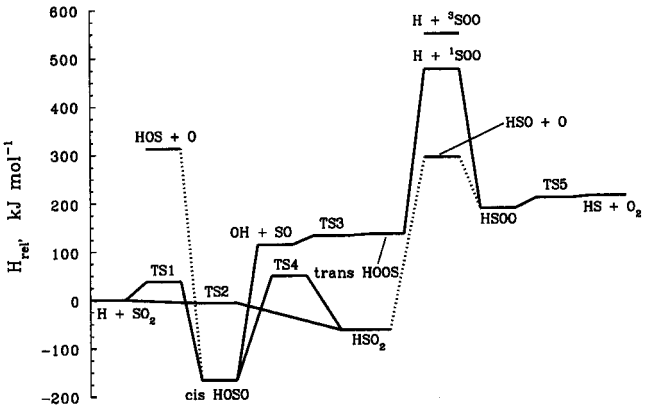

Figure 3. Potential energy diagram calculated at the G2 level, showing enthalpies at 0 K relative to H + SO_2.

TABLE 3: Thermochemical Data for HSO_2

T K	C_p J K^{-1} mol^{-1}	S J K^{-1} mol^{-1}	$H_T - H_0$ kJ mol^{-1}	$\Delta_f H°$ kJ mol^{-1}	$\Delta_f G°$ kJ mol^{-1}
200	38.4	247.3	6.9	−139.1	−133.2
298.15	44.4	263.7	11.0	−141.4	−129.9
400	50.6	277.7	15.8	−145.7	−125.5
500	56.0	289.6	21.2	−148.8	−120.1
700	64.1	309.8	33.2	−153.1	−107.8
1000	71.4	334.0	53.7	−208.6	−80.6
1300	75.4	353.3	75.8	−206.2	−41.1
2000	79.5	386.8	130.2	−204.0	45.9

TABLE 4: Thermochemical Data for *cis*-HOSO

T K	C_p J K^{-1} mol^{-1}	S J K^{-1} mol^{-1}	$H_T - H_0$ kJ mol^{-1}	$\Delta_f H°$ kJ mol^{-1}	$\Delta_f G°$ kJ mol^{-1}
200	49.0	262.0	8.3	−240.1	−237.1
298.15	53.4	282.3	13.3	−241.4	−235.3
400	57.1	298.6	19.0	−244.9	−233.0
500	60.1	311.7	24.8	−247.5	−229.8
700	64.3	332.6	37.3	−251.3	−222.0
1000	68.3	356.3	57.3	−307.3	−201.2
1300	71.1	374.6	78.2	−307.3	−169.8
2000	74.7	406.0	129.4	−307.2	−95.8

the reaction coordinate (the length of the breaking bond), fitted to a Morse potential, were selected, and the point that gave the smallest k_∞, taking angular momentum barriers into account, was taken as the best estimate of the rate constant. Typically a "loose" TS was located, where the breaking bond is extended to several times the equilibrium length.[43] This kind of TS may be analyzed in terms of the Gorin model[43,50] as a loose adduct of the two separating fragments, with a set of vibrational modes equal to those of the fragments. The independent rotational modes of the separated fragments correlate to rocking and torsional motions about the stretched partial bond in the TS, and these modes were incorporated into the Gorin model as internal rotors. Energy transfer was estimated as outlined for

TABLE 5: Thermochemical Data for HSOO

T K	C_p J K^{-1} mol^{-1}	S J K^{-1} mol^{-1}	$H_T - H_0$ kJ mol^{-1}	$\Delta_f H°$ kJ mol^{-1}	$\Delta_f G°$ kJ mol^{-1}
200	46.0	263.6	8.2	113.0	115.7
298.15	51.7	283.0	13.0	111.5	117.3
400	56.8	299.0	18.5	107.9	119.6
500	60.5	312.1	24.4	105.3	122.8
700	65.6	333.3	37.1	101.7	130.5
1000	70.2	357.5	57.5	46.1	150.7
1300	72.9	376.3	79.0	46.7	181.9
2000	76.0	408.5	131.3	47.9	254.5

TABLE 6: RRKM Input Parameters for Loose Transition States

TS	$r^\dagger$ Å[a]	ν cm^{-1}	B_{int}(active) cm^{-1} [b]	B_{ext}(active) cm^{-1} [b]	B_{ext}(inactive) cm^{-1} [b]
HS···O_2 (5)	≈2.6	2641	9.935, 2	1.662, 1	0.166, 2
		1343	10.26, 1		
HO···SO (6)	≈5.0	3556	17.91, 2	0.797, 1	0.474, 2
		1049	19.61, 1		
HSO···O (11)	≈2.7	2418	0.223, 2	1.111, 1	0.117, 2
		1170			
		1017			

[a] Variationally determined separation at 298 K. [b] Rotational constants and dimensions for internal rocking and/or torsions and overall external rotations. The symmetry numbers for all rotations are 1.

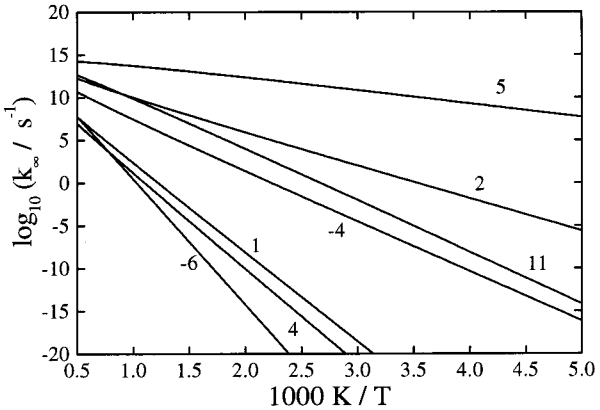

Figure 4. Arrhenius plot of high-pressure limits of dissociation/isomerization reactions: (1) HOSO → H + SO_2; (2) HSO_2 → H + SO_2; (4,−4) HOSO ⇌ HSO_2; (5) HSOO → SH + O_2; (−6) HOSO → OH + SO; (11) HSOO → HSO + O.

method A. The absence of a barrier means no tunneling correction was required.

The input parameters for the kinetic calculations are listed in Table 6. The temperature and pressure dependence of the predicted rate constants are shown in Figures 4−8, and Table 7 summarizes the low- and high-pressure limits in the form $A\,T^B \exp(-C/T)$. Individual reactions are now discussed in more detail.

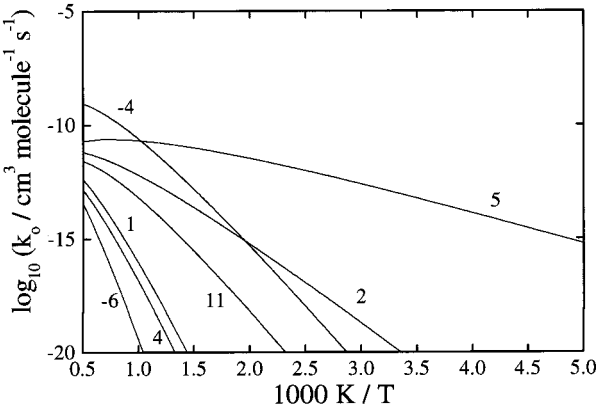

Figure 5. Arrhenius plot of low-pressure limits of dissociation/isomerization reactions, numbered as in Figure 4.

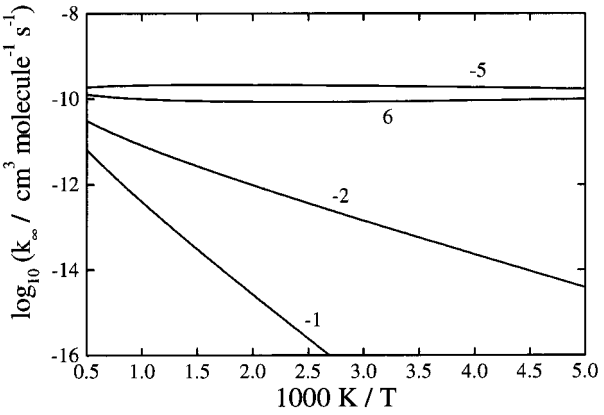

Figure 6. Arrhenius plot of high-pressure limits of recombination reactions: (−1) H + SO_2 → HOSO; (−2) H + SO_2 → HSO_2; (−5) SH + O_2 → HSOO; (6) OH + SO → HOSO.

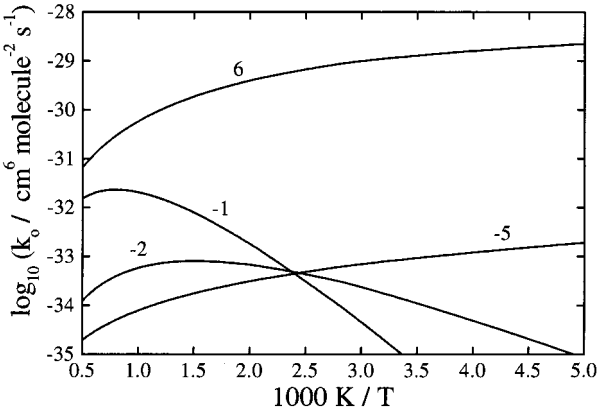

Figure 7. Arrhenius plot of low-pressure limits of recombination reactions numbered as in Figure 6.

III.3.1 Reactions Involving HOSO. The addition of H to SO_2 to form HOSO, reaction −1, is unusual because of the large predicted barrier; most recombination reactions have no barrier and proceed with zero or slightly negative activation energies.[51] The high degree of spin contamination in the HF/6-311G(d,p) wave function of TS1 led us to reoptimize its geometry at the QCISD level, with the main consequence that the partial O−H bond was lengthened from 1.51 to 1.61 Å (see Figure 2), which decreased the G2 energy by only about 3 kJ mol^{-1}. The significant barrier to reaction −1 also means that quantum mechanical tunneling may be important; equation 12 yields $\Gamma = 2.23$ at 700 K, decreasing to 1.15 at 2000 K. Figure 8 illustrates the pressure dependence of k_1 and shows that at ambient conditions the reaction is expected to lie close to the high-pressure limit, although it would be too slow to observe (see Figure 6). At higher temperatures, the kinetics approach the low-pressure limit. Fenimore and Jones obtained a value of $k_{o,-1}$ of 1.9×10^{-31} cm^6 $molecule^{-1}$ s^{-1} at 784 K in the postcombustion region of an H_2/O_2 flame,[52] 15 times larger than our calculated value (Table 7) of 1.3×10^{-32} cm^6 $molecule^{-1}$ s^{-1}, which may reflect uncertainties in their flame model, some of which are discussed below. At 500 K the calculated result $k_{o,-1} = 1.9 \times 10^{-33}$ cm^6 $molecule^{-1}$ s^{-1} is in better accord with the experimental upper limit, obtained when this reaction was isolated in our laboratory, of 1.5×10^{-33} cm^6 $molecule^{-1}$ s^{-1}.[16]

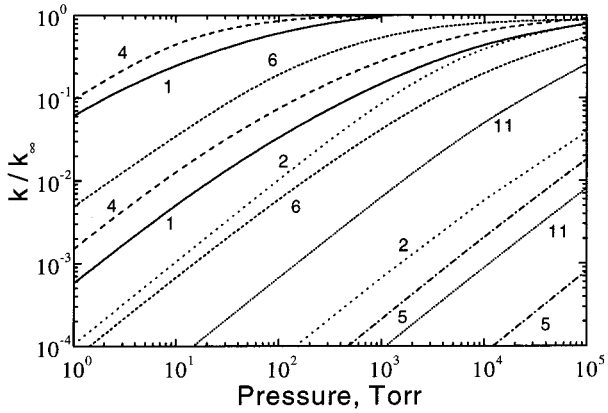

Figure 8. Falloff curves for unimolecular reactions: (1) HOSO → H + SO_2, solid line; (2) HSO_2 → H + SO_2, dotted line; (4) HOSO → HSO_2, dashed line; (5) HSOO → HS + O_2, dots and dashes; (6) HO + SO → HOSO, short dashed line; (11) HSOO → HSO + O, small dots. Upper and lower curves are for 298 and 1000 K, respectively.

As outlined in the Introduction, this reaction may be important in sulfur-containing flames because HOSO could be removed quickly in a subsequent step, such as reaction with H, so that the net effect is to catalyze H + H → H_2, which is otherwise fairly slow under combustion conditions. Quantitative flame models typically are sensitive to the product of the equilibrium constant for reaction −1, $K_{eq,-1}$, and the bimolecular rate constant that characterizes removal of the adduct by H atoms, $k_{removal}$,[53] which is an effective third-order rate constant for H atom consumption. We calculate $K_{eq,-1} = 1.2 \times 10^{-19}$ cm^3 $molecule^{-1}$ at 2000 K, which is much lower than previous values used in flame models that were based on $\Delta H = 264$ kJ mol^{-1} for reaction 1.[53] If $k_{removal} \approx 5 \times 10^{-11}$ cm^3 $molecule^{-1}$ s^{-1}, then our $K_{eq,-1}$ is compatible with the earlier flame values for the product $K_{eq,-1}k_{removal}$.[53] This value of $k_{removal}$ is plausible, especially given the order of magnitude of uncertainty in the flame kinetic data, and is similar to the recommended rate constant for H + HNO of 2.3×10^{-11} cm^3 $molecule^{-1}$ s^{-1}.[54] Thus, our revised H−OSO bond strength obtained ab initio is compatible with the earlier flame observations.

The recombination reaction 6, OH + SO → HOSO, has no barrier and therefore is fast (see Figure 7). At room temperature and atmospheric pressure, the effective second-order rate constant is 0.4 of k_∞, in the middle of the falloff regime (see Figure 8). However, because HOSO is intially formed with sufficient energy to dissociate to H + SO_2, formation of stabilized HOSO is probably a minor channel except at very high [M], and the overall consumption of OH by SO is predicted to be given by $k_{\infty,6} = 1.9 \times 10^{-10}$ cm^3 $molecule^{-1}$ s^{-1}, with H + SO_2 as major products. According to Pauwels et al., this is the dominant route for SO_2 formation in a methanol flame doped with H_2S.[55] The theoretical value is in reasonable accord with measurements of the total OH + SO rate constant of 8.6 ×

TABLE 7: Rate Constant Expressions in the Form $k = AT^B \exp(-C/T)$[a]

	low-pressure limit			high-presure limit		
reaction	*A*	*B*	*C*	*A*	*B*	*C*
HOSO → H + SO_2 (1)	2.58×10^{7}	−4.53	24750	1.70×10^{10}	0.80	23620
H + SO_2 → HOSO (−1)	5.78×10^{-17}	−4.36	5440	3.85×10^{-14}	0.96	4320
HSO_2 → H + SO_2 (2)	5.74×10^{1}	−3.29	9610	2.03×10^{11}	0.90	9240
H + SO_2 → HSO_2 (−2)	7.74×10^{-22}	−3.69	2410	6.74×10^{-13}	0.62	1820
HOSO → HSO_2 (4)	2.86×10^{11}	−5.64	27890	1.03×10^{9}	1.03	25150
HSO_2 → HOSO (−4)	2.88×10^{11}	−5.31	15750	1.62×10^{9}	1.31	13060
HSOO → SH + O_2 (5)	2.59×10^{-1}	−2.82	−3750	4.41×10^{18}	−1.07	3900
SH + O_2 → HSOO (−5)	8.52×10^{-29}	−2.01	10	1.45×10^{-9}	−0.26	150
OH + SO → HOSO (6)	2.63×10^{-20}	−3.48	490	2.59×10^{-12}	0.50	−200
HOSO → OH + SO (−6)	2.07×10^{8}	−4.33	34780	1.65×10^{16}	−0.32	34080
HSOO → HSO + O (11)	1.54×10^{11}	−5.87	15580	2.01×10^{19}	−1.07	14280

[a] Units are s^{-1} for first-order reactions, cm^3 $molecule^{-1}$ s^{-1} for second-order reactions, and cm^6 $molecule^{-2}$ s^{-1} for third-order reactions.

10^{-11} cm^3 $molecule^{-1}$ s^{-1} (with a recommended uncertainty of factor of 2).[56]

Once HOSO is formed, the two most favorable pathways for its unimolecular decomposition are (1), discussed above, and (4), isomerization to less stable HSO_2. These pathways have similar energy barriers and similarly tight TSs, and thus comparable rate constants (see Figures 4 and 5). These loss processes are slow below about 700 K, and therefore HOSO should be an isolable species. As may be seen from Figures 4 and 5, we predict $k_1 > k_4$ at both the high- and low-pressure limits. Qi et al. argued the opposite case, but their neglect of tunneling effects which are greater for k_1, and use of MP2 energies which, because TS1 has greater spin contamination than TS4, will overestimate the barrier to reaction 1 as compared to reaction 4, make their conclusion suspect.[24] At high temperatures, HSO_2 will rapidly dissociate to H + SO_2 (see following section), so both pathways have similar impacts on combustion chemistry.

III.3.2. Reactions Involving HSO_2. There are apparent discrepancies between experimental studies of H + SO_2 recombination, reaction −2. Gordon et al.[57] observed shifts and broadening of hyperfine lines in the microwave spectrum of atomic hydrogen induced by collisions with SO_2 and derived a total rate constant for formation of an excited adduct of 3×10^{-13} cm^3 $molecule^{-1}$ s^{-1}. This should correspond to the high-pressure limit $k_{\infty,-2}$. On the other hand, Fair and Thrush[58] and Binns and Marshall[16] observed no reaction between H and SO_2 in fast-flow/chemiluminescence and flash-photolysis/resonance fluorescence experiments.

The G2 energy for TS2 at the MP2/6-31G(d) geometry listed in Table 2 is 7.0 kJ mol^{-1} below H + SO_2, implying no barrier to the recombination. As noted earlier, unrealistic MP2 frequencies indicate that TS2 is not properly described at this level, so we reoptimized the geometry at the QCISD/6-311G(d,p) level. The new geometry has an extended S−H separation of 2.11 Å, with the other parameters little changed (see Figure 2).The revised G2 energy is 8.9 kJ mol^{-1} above H + SO_2. We analyzed TS2 at the QCISD/6-311G(d,p) level as a tight transition state in method A and included a Wigner tunneling correction to obtain $k_{\infty,-2} = 5.2 \times 10^{-14}$ cm^3 $molecule^{-1}$ s^{-1} at room temperature, which lies moderately near the value proposed by Gordon et al.[57] The recombination process is close to the low-pressure limit at typical experimental pressures of 100 Torr or less (see Figure 8), and $k_{o,-2}$ is calculated to be about 1.8×10^{-34} cm^6 $molecule^{-2}$ s^{-1} at 298 K, below the experimental upper limits.[16,58] Thus, most of the kinetic measurements can be rationalized by the computational analysis. We note that our value for $k_{o,-2}$ is about 6 times smaller than that proposed by Gordon et al.,[57] implying a shorter lifetime for initially excited HSO_2 than they found.

An alternative explanation of the lack of observed H + SO_2 reactivity might be that HSO_2 is loosely bound so that once formed it rapidly dissociates at room temperature to regenerate H. We can test this idea using the equilibrium constant $K_{eq,-2} = 2.6 \times 10^{-14}$ cm^3 $molecule^{-1}$ at 298 K, calculated from the data of Table 3. For typical experimental conditions of $[SO_2] = 10^{15}$ molecules $cm^{-3} \gg$ [H], the equilibrium ratio $[HSO_2]$:[H] is 26; that is, most of the H atoms would be consumed. Thus, we suggest the lack of observed H + SO_2 addition at 298 K reflects a small rate constant, rather than unfavorable thermochemistry. Higher temperatures increase the third-order rate constant somewhat (see Figure 7), because the barrier becomes less significant relative to RT, but at the same time collisional stabilization efficiency and the equilibrium constant decrease, so there are no conditions predicted to be favorable for direct observation of reaction −2 at low pressures. The theoretical data indicate that HSO_2 is the kinetically favored product of H + SO_2 at lower temperatures, while at higher temperatures the thermodynamic product HOSO will dominate. For example, at 2000 K, $K_{eq,-2}$ is about 500 times smaller than $K_{eq,-1}$, so formation of HSO_2 is likely to be negligible compared to HOSO in sulfur-seeded flames.

As noted in section III.2, HSO_2 is a thermochemically allowed product of the reactions of HSO with NO_2, N_2O, and O_3, so it may participate in the atmospheric chemistry of sulfur. We estimate the lifetime of HSO_2 at 1 atm pressure with respect to dissociation to be about 13 s at 298 K and 130 s at 273 K. While the exact numbers depend on the particular H−SO_2 bond strength and tunneling model employed, they illustrate a strong temperature sensitivity of SO_2 production via HSO oxidation, which may need to be taken into account in atmospheric models.

III.3.3. HSOO Reactions. HSOO is predicted to be weakly bound, by about 31 kJ mol^{-1},[19] so that the SH + O_2 recombination reaction, controlled by passage through TS5, will only be important close to room temperature or below. There is high spin contamination in the underlying HF wave function for TS5 (see Table 2), which should largely be corrected by the QCI component of the G2 procedure. Any residual errors will make the energy too positive, but TS5 is already calculated to fall about 3 kJ mol^{-1} below SH + O_2 at the MP2/6-31G(d) geometry. Spin contamination makes this geometry suspect, so we reoptimized TS5 at the QCISD/6-311G(d,p) level. The G2 energy of this new structure is 1 kJ mol^{-1} below SH + O_2. Accordingly, we analyzed HSOO dissociation in terms of a loose TS defined by a rotational barrier. Our kinetics analysis (Figure 8) suggests reaction −5 lies close to the low-pressure limit, even at 1 atm and 250 K. The implications for atmospheric chemistry have been discussed elsewhere;[25] briefly, reaction −5 is likely to be the fastest pathway for atmospheric SH oxidation, provided the temperature is low enough for the thermochemistry to be

favorable. Under the higher temperatures relevant to combustion, the equilibrium [HSOO] will be negligible.

HSOO is a potential transient intermediate in the flame oxidation of SH to HSO. The results of RRKM calculations of k_{11}, based on the assumption that there is no barrier beyond the endothermicity for HSOO dissociation to HSO + O, are shown in Figures 4 and 5. We found that k_{11} is close to the low-pressure limit at pressures up to 2000 Torr at all temperatures. The bottleneck in the pathway SH + O_2 → HSOO → HSO + O, which has an overall G2 ΔH_0 of 81 kJ mol^{-1}, is the loose TS for breaking the O−O bond in HSOO; thus, the effective second-order rate constant for HSO formation from SH + O_2 is the product of the equilibrium constant for HSOO formation and $k_{\infty,11}$, 8.1×10^{-10} exp(−10250K/T) cm^3 molecule^{-1} s^{-1} for the temperature range 700−2000 K. This pathway may be significant in combustion because it leads to an important intermediate; we predicted earlier that HSO is labile with respect to atomic hydrogen and it is also likely to react quickly with other radicals.[34,59]

Another pathway for SH + O_2 in flames would be formation of HO_2 + S, but these products are unlikely because they are about 60 kJ mol^{-1} more endothermic than HSO + O. Formation of OH + SO is 99 kJ mol^{-1} exothermic relative to SH + O_2, but a four-center TS with extensive bond rearrangements would be needed for this to be an elementary process. Isomerization of HSOO to an HOOS-like geometry followed by O−O fission provides a more plausible pathway. Our searches so far of the PES (Figure 3) have not defined a TS for HSOO isomerization but indicate that if it exists it has a similar energy to H + SOO, which would imply a barrier to isomerization of around 250 kJ mol^{-1}. We therefore suggest that HSO + O are the most likely initial products of SH + O_2 at high temperatures.

IV. Conclusions

Reaction pathways for unimolecular processes on the H/S/O/O potential energy surface have been characterized by ab initio methods, and the kinetics were predicted by means of RRKM theory. Where comparisons can be made, there is generally good accord between calculations and measurements. Thermochemical and kinetic data at high- and low-pressure limits are tabulated. HOOS is suggested to be unbound with respect to OH + SO, and possible reactions leading to and from HSOO, HSO_2, and HOSO are considered. A revised theoretical H−OSO bond strength is found to be compatible with flame data on catalysis of H + H recombination by SO_2. Disagreements between different experimental studies of H + SO_2 → HSO_2 are largely resolved by a mechanism that involves a modest barrier to recombination, while some implications of the reverse process for the atmospheric lifetime of HSO_2 and formation of SO_2 are discussed. An effective second-order rate constant for SH + O_2 → HSO + O proceeding via an HSOO intermediate under flame conditions has been derived.

Acknowledgment. We thank Prof. John Stanton at The University of Texas at Austin for valuable discussions and calculations concerning the wave function instability of TS2. J.-D.R.R. is grateful to the Ronald E. McNair Post-Baccalaureate Achievement Program for a scholarship. This work was supported by the Robert A. Welch Foundation (Grant B-1174) and the UNT Faculty Research Fund, and computer time was provided through the NSF Pittsburgh Supercomputing Center (Grant CHE900059P) and the Materials Directorate of the Air Force Research Laboratory at Wright-Patterson AFB, Ohio.

Supporting Information Available: Figure 1S contains diagrams of atomic displacements for the normal modes of the transition states. This material is available free of charge via the Internet at http://pubs.acs.org.

References and Notes

(1) McDowell, C. A.; F. G. Herring, F. G.; Tait, J. C. *J. Chem. Phys.* **1975**, *63*, 3278.
(2) Zacharia, M. R.; Smith, O. I. *Combust. Flame* **1987**, *69*, 125.
(3) Kallend, A. S. *Trans. Faraday Soc.* **1967**, *63*, 2442.
(4) Halstead, C. J.; Jenkins, D. R. *Trans. Faraday Soc.* **1969**, *65*, 3013.
(5) Drurie, R. A.; Johnson, G. M.; Smith, M. Y. *Combust. Flame* **1971**, *17*, 197.
(6) Cullis, C. F.; Mulcahy, M. F. R. *Combust. Flame* **1972**, *18*, 225.
(7) Kallend, A. S. *Combust. Flame* **1972**, *19*, 227.
(8) Lovejoy, E. R.; Wang, N. S.; Howard, C. J. *J. Phys. Chem.* **1987**, *91*, 5749.
(9) Lee, Y.-Y.; Lee, Y.-P.; Wang, N. S. *J. Chem. Phys.* **1994**, *100*, 387.
(10) Frank, A. J.; Sadílek, M.; Ferrier, J. G.; Tureček, F. *J. Am. Chem. Soc.* **1996**, *118*, 11321.
(11) Frank, A. J.; Sadílek, M.; Ferrier, J. G.; Tureček, F. *J. Am. Chem. Soc.* **1997**, *119*, 12343.
(12) Turnipseed, A. A.; Barone, S. B.; Ravishankara, A. R. *J. Phys. Chem.* **1992**, *96*, 7502.
(13) Morris, V. R.; Han, K.-L.; Jackson, W. M. *J. Phys. Chem.* **1995**, *99*, 10086.
(14) Boyd, R. J.; Gupta, A.; Langler, R. F.; Lownie, S. P.; Pincock, J. A. *Can. J. Chem.* **1980**, *58*, 331.
(15) Hinchliffe, A. *J. Mol. Struct. (THEOCHEM)* **1981**, *71*, 349.
(16) Binns, D.; Marshall, P. *J. Chem. Phys.* **1991**, *95*, 4940.
(17) Basch, H.; Hoz, T. In *The Chemistry of Sulphonic Acids, Esters and their Derivatives*; Patai, S., Rappoport, Z., Eds.; Wiley: London, 1991; Chapter 1.
(18) Morris, V. R.; Jackson, W. M. *Chem. Phys. Lett.* **1994**, *223*, 445.
(19) Laakso, D.; Smith, C. E.; Goumri, A.; Marshall, P. *Chem. Phys. Lett.* **1994**, *227*, 377.
(20) Pople, J. A.; Head-Gordon, M.; Fox, D. J.; Raghavachari, K.; Curtiss, L. A. *J. Chem. Phys.* **1989**, *90*, 5622.
(21) Curtiss, L. A.; Jones, C.; Trucks, G. W.; Raghavachari, K.; Pople, J. A. *J. Chem. Phys.* **1990**, *93*, 2537.
(22) Curtiss, L. A.; Raghavachari, K.; Trucks, G. W.; Pople, J. A. *J. Chem. Phys.* **1991**, *94*, 7221.
(23) Glarborg, P.; Kubel, D.; Dam-Johansen, K.; Chiang, H.-M.; Bozzelli, J. W. *Int. J. Chem. Kinet.* **1996**, *28*, 773.
(24) Qi, J.-X.; Deng, W.-Q.; Han, K.-L.; He, G.-Z. *J. Chem. Soc., Faraday Trans.* **1997**, *93*, 25.
(25) Goumri, A.; Rocha, J.-D. R.; Marshall, P. *J. Phys. Chem.* **1995**, *99*, 10834.
(26) Hehre, W. J.; Radom, L.; Schleyer, P. v. R.; Pople, J. A. *Ab Initio Molecular Orbital Theory*; Wiley: New York, 1986.
(27) Foresman, J. B.; Frisch, Æ. *Exploring Chemistry with Electronic Structure Methods*; Gaussian, Inc.: Pittsburgh, 1993.
(28) Frisch, M. J.; Head-Gordon, M.; Truck, G. W.; Foresman, J. B.; Schlegel, H. B.; Raghavachari, K.; Robb, M. A.; Binkley, J. S.; Gonzalez, C.; Defrees, D. J.; Fox, D. J.; Whiteside, R. A.; Seeger, R.; Melius, C. F.; Baker, J.; Martin, R. L.; Kahn, L. R.; Stewart, J. J. P.; Topiol, S.; Pople, J. A. *Gaussian 90*; Gaussian, Inc.: Pittsburgh, 1990.
(29) Frisch, M. J.; Truck, G. W.; Head-Gordon, M.; Gill, P. M. W.; Wong, M. W.; Foresman, J. B.; Johnson, B. G.; Schlegel, H. B.; Robb, M. A.; Replogle, E. S.; Gomperts, R.; Andres, J. L.; Raghavachari, K.; Binkley, J. S.; Gonzalez, C.; Martin, R. L.; Fox, D. J.; Defrees, D. J.; Baker, J.; Stewart, J. J. P.; Pople, J. A. *Gaussian 92*; Gaussian, Inc.: Pittsburgh, 1992.
(30) Frisch, M. J.; Truck, G. W.; Schlegel, H. B.; Gill, P. M. W.; Johnson, B. G.; Robb, M. A.; Cheeseman, J. R.; Keith, T.; Petersson, G. A.; Montgomery, J. A.; Raghavachari, K.; Al-Laham, M. A.; Zakrzewski, V. G.; Ortiz, J. V.; Foresman, J. B.; Cioslowski, J.; Stefanov, B. B.; Nanayakkara, A.; Challacombe, M.; Peng, C. Y.; Ayala, P. Y.; Chen, W.; Wong, M. W.; Andres, J. L.; Replogle, E. S.; Gompert, R.; Martin, R. L.; Fox, D. J.; Binkley, J. S.; Defrees, D. J.; Baker, J.; Stewart, J. J. P.; Head-Gordon, M.; Gonzalez, C.; Pople, J. A. *Gaussian 94*, revision D2; Gaussian, Inc.: Pittsburgh, 1995.
(31) Pople, J. A.; Scott, A. P.; Wong, M. W.; Radom, L. *Isr. J. Chem.* **1993**, *33*, 345.
(32) Seeger, R.; Pople, J. A. *J. Chem. Phys.* **1977**, *66*, 3045.
(33) Durant, J. L., Jr.; Rohlfing, C. M. *J. Chem. Phys.* **1993**, *98*, 8031.
(34) Goumri, A.; Rocha, J.-D. R.; Laakso, D.; Smith, C. E.; Marshall, P. J. *Chem. Phys.* **1994**, *101*, 9405.
(35) Crawford, T. D.; Stanton, J. F.; Allen, W. D.; Schaefer, H. F., III *J. Chem. Phys.* **1997**, *107*, 10626.
(36) Calculations carried out by Stanton, J. F. using a local version of the ACES II program (see the following reference).
(37) Stanton, J. F.; Gauss, J.; Watts, J. D.; Lauderdale, W. J.; Bartlett, R. J. *Int. J. Quantum Chem.* **1992**, *Symp. 26*, 879.

(38) Apparent TS structures, with single imaginary frequencies, yielded unusual discrepancies between results obtained with implementations of GAUSSIAN software on different computers in these cases only.

(39) Chase, M. W., Jr.; Davies, C. A.; Downey, J. J. R.; Frurip, D. J.; McDonald, R. A.; Syverud, A. N. *JANAF Thermochemical Tables*, 3rd ed.; American Institute of Physics: Woodbury, NY, 1985; Suppl. 1, Vol. 14.

(40) The bond dissociation energies of O−O_2, O−NO, and O−N_2 are 101.4, 161.3, and 300.6 kJ mol^{-1}, respectively (see ref 39). The strengths of the HSO−O bond and the S−O bond in HSO_2 are 127.2 and 378.1 kJ mol^{-1}, respectively (see ref 19).

(41) Gilbert, R. G.; Smith, S. C. *Theory of Unimolecular and Recombination Reactions*; Blackwell: Oxford, UK, 1990.

(42) Gilbert, R. G.; Jordan, M. J. T.; Smith, S. C. UNIMOL Sydney, Australia, 1990 (see preceding reference).

(43) Benson, S. W. *Thermochemical Kinetics*, 2nd ed.; Wiley: New York, 1976; Chapter 3.

(44) McKee, R. J.; Dixon-Lewis, G.; Warnatz, J.; Coltrin, M. E.; Miller, J. A. Sandia Report SAND86-8246, 1986.

(45) Mulcahy, M. F. R. *Gas Kinetic*; Nelson: London, 1973.

(46) *TRC Thermodynamic Tables: Non-Hydrocarbons*; Thermodynamics Research Center, The Texas A & M University System: College Station, TX, 1987; p 280.

(47) Nicovich, J. M.; Kreutter, K. D.; van Dijk, C. A.; Wine, P. H. *J. Phys. Chem.* **1992**, *96*, 2518.

(48) Nourbakhsh, S.; Norwood, K.; Yin, H.-M.; Liao, C.-L.; Ng, C. Y. *J. Chem. Phys.* **1991**, *95*, 946.

(49) Continetti, R. E.; Balko, B. A.; Lee, Y. T. *Chem. Phys. Lett.* **1991**, *182*, 400.

(50) Gorin, E. *Acta Physiochim. URSS* **1989**, *9*, 691.

(51) Tröe, J. In *Reactions of Small Transient Species*; Fontijn, A., Clyne, M. A. A., Eds.; Academic: London, 1983; Chapter 2.

(52) Fenimore, C. P.; Jones, G. W. *J. Phys. Chem.* **1965**, *69*, 3593.

(53) Baulch, D. L.; Drysdale, D. D.; Duxbury, J.; Grant, S. J. *Evaluated Kinetic Data for High-Temperature Reactions*; Butterworth: London, 1976; Vol. 3.

(54) Tsang, W.; Herron, J. T. *J. Phys. Chem. Ref. Data* **1991**, *20*, 609.

(55) Pauwels, J. F.; Carlier, M.; Devolder, P.; Sochet, L. R. *Combust. Sci. Technol.* **1992**, *86*, 237.

(56) DeMore, W. B.; Sander, S. P.; Golden, D. M.; Hampson, R. F.; Kurylo, M. J.; Howard, C. J.; Ravishankara, A. R.; Kolb, C. E.; Molina, M. J. *Chemical Kinetics and Photochemical Data for Use in Stratospheric Modeling. Evaluation 12*; JPL Publication 97-4; NASA Jet Propulsion Laboratory: Pasadena, 1997.

(57) Gordon, E. B.; Ivanov, B. I.; Perminov, A. P.; Balalaev, V. E. *Chem. Phys.* **1978**, *35*, 79.

(58) Fair, R. W.; Thrush, B. A. *Trans. Faraday Soc.* **1969**, *65*, 1550.

(59) Goumri, A.; Rocha, J.-D. R.; Laakso, D.; Smith, C. E.; Marshall, P. *J. Chem. Phys.* **1995**, *102*, 161.